 CMES, vol.21, no.3, pp.177-191, 2007

# Geometrically Nonlinear Analysis of Reissner-Mindlin Plate by Meshless Computation

**P. H. Wen**[1] **and Y. C. Hon**[2]

**Abstract:** In this paper, we perform a geometrically nonlinear analysis of Reissner-Mindlin plate by using a meshless collocation method. The use of the smooth radial basis functions (RBFs) gives an advantage to evaluate higher order derivatives of the solution at no cost on extra-interpolation. The computational cost is low and requires neither the connectivity of mesh in the domain/boundary nor integrations of fundamental/particular solutions. The coupled nonlinear terms in the equilibrium equations for both the plane stress and plate bending problems are treated as body forces. Two load increment schemes are developed to solve the nonlinear differential equations. Numerical verifications are given to demonstrate the efficiency and accuracy of the proposed method in comparing with exact solutions and results from using the finite element software (ABAQUS).

**Keyword:** large deformation, Reissner-Mindlin plate theory, meshless collocation, radial basis functions.

## 1 Introduction

The theory developed for Reissner-Mindlin plate with shear deformation plays an important role in the engineering industries such as aircraft and ship constructions. It is well known that if the deflection of a plate is of the order of the thickness, the effect of the fourth-order derivatives for the deflection for plate bending and displacement for in-plane problem has to be included into the governing partial differential equations. The classical thin plate theory of Kirchhoff gives rise to certain non-physical simplification from the omission of the shear deformations and rotary inertia, which are significant for higher thickness of the plate. The Reissner-Mindlin plate bending theory [Reissner (1945), Mindlin (1951)] takes care of the effects of shear deformation and rotary inertia. The solution for Reissner's plate model was first given by Vander Ween (1982) using the boundary integral equation method. Recently, Wen and Aliabadi (2005) applied displacement discontinuity method for cracked Reissner's plates.

For the geometrically nonlinear analysis of thin and moderately thick plates, one of the difficulties is to evaluate domain integrals in the boundary integral equations. A cell technique similar to finite element was studied by Lei et al (1990). Since the cell technique has to mesh the domain to evaluate these domain integrals, the advantage of the boundary element method that reduces the dimension of the problem is compromised from this point of view. To transform these domain integrals into the boundary integrals, dual reciprocity method proposed by Nardini and Brebbia (1982) was used for thick plate problems by Wang and Tanaka (2000).

Numerical solutions of partial differential equations are commonly obtained by the use of finite difference method (FDM), finite element method (FEM) and boundary element method (BEM). The FDM involves a rectangular grid system and has difficulties in representing irregular domain problems. Since finite difference grids and meshed elements are needed in the numerical procedures of FDM and FEM respectively, they both belong to the mesh-dependent category that has been widely used in computational fluid dynamics (CFD). In the last decade, the development of meshless methods has shown to provide a promising alternative to the finite element and bound-

[1] Department of Engineering, Queen Mary, University of London, UK

[2] Corresponding author. Department of Mathematics, City University of Hong Kong, HKSAR, China

ary element methods for solving differential equations. There are basically two types of meshless computational methods: weak formulation type and strong collocation type. The weak formulation type meshless approximations have received much attention since the works of Nayroles et al(1992) who proposed the diffuse element method and Belyschko et al (1994) and Liu et al (1995) who proposed element-free Galerkin method and reproducing kernel particle methods, respectively. A key feature of these methods is that they do not require any structured grid and are hence meshless in nature. Recently, Atluri and his colleagues presented a family of Meshless methods based on the local weak Petrov-Galerkin formulation (MLPGs) for arbitrary partial differential equations [Atluri and Zhu (1998a,b), Atluri and Shen (2000), Atluri (2004)] with moving least-square (MLS) approximation technique. The MLPG has been reported to provide a rational basis for constructing meshless methods with a greater degree of flexibility. Recently, the Local Boundary Integral Equation method (LBIE) with MLS and polynomial radial function has been developed by Sladek et al (2004a, 2004b, 2005) for solving boundary value problems in anisotropic non-homogeneous media. Both methods (MLPG and LBIE) are meshless as no domain/boundary meshes are required in these two approaches. However, Galerkin-based meshless methods except MLGP presented in Atluri and Zhu (1998a) by Atluri still include some awkward implementation features such as numerical integrations in the local domain. A comprehensive review of meshless methods (MLPG) can be found in Atluri and Zhu (1998a). For the continuous model, Chen et al (2006) used the null-field integral equation, Fourier series and the series expansion in terms of degenerate kernel for fundamental solutions to examine the solvability of BIEM for circular thin plates.The MLPG has been reported to provide a rational basis for constructing meshless methods with a greater degree of flexibility. Recently, the Local Boundary Integral Equation method (LBIE) with MLS and polynomial radial function has been developed by Sladek et al (2004a, 2004b, 2005) for solving boundary value problems in anisotropic non-homogeneous media. Both methods (MLPG and LBIE) are meshless as no domain/boundary meshes are required in these two approaches. However, Galerkin-based meshless methods except MLGP presented in Atluri and Zhu (1998a) by Atluri still include some awkward implementation features such as numerical integrations in the local domain. A comprehensive review of meshless methods (MLPG) can be found in Atluri Atluri and Zhu (1998a). The strong collocation type meshless computational method was first introduced by Kansa (1990) and later improved by Hon et al (1999), Hon and Wu (2000), for solving various kinds of partial differential equations including inverse problems. For the continuous model, Chen et al (2006) used the null-field integral equation, Fourier series and the series expansion in terms of degenerate kernel for fundamental solutions to examine the solvability of BIEM for circular thin plates

The strong collocation type meshless computational method using radial basis functions was first introduced by Kansa (1990) and later improved by Hon et alHon et al (1999), Hon and Wu (2000), for solving various kinds of partial differential equations. The method has recently successfully extended to solve, for instances, problems in laminated composite plates [Mai-Duy (2007a), Hon et al (1005)]; transient viscous flows [Mai-Cao and Tran-Cong (2005), Mai-Duy et al (2007b)]; incompressible Navier-Stokes and cavity fluid flows [Šarler (2005), Chantasiriwan (2006), Shu et al (2005)]; Maxell's equation [Young et al (2006)]; elastro-thermo-viscoplastic material (Le et al (2007)) and time dependent heat transfer [La Rocca et al (2005)].

In the present paper we further extend the meshless collocation method to develop a geometrically nonlinear analysis for large deformation of plate bending problems. Since the meshless collocation method computes the solution entirely based on collocation points instead of elements in the conventional FEM or BEM, the proposed approach overcomes the difficulty in the determination of high order derivatives of the shape functions by using an indirect scheme and two load schemes. This provides the advantage to treat the coupling nonlinear effects of in-plane stress

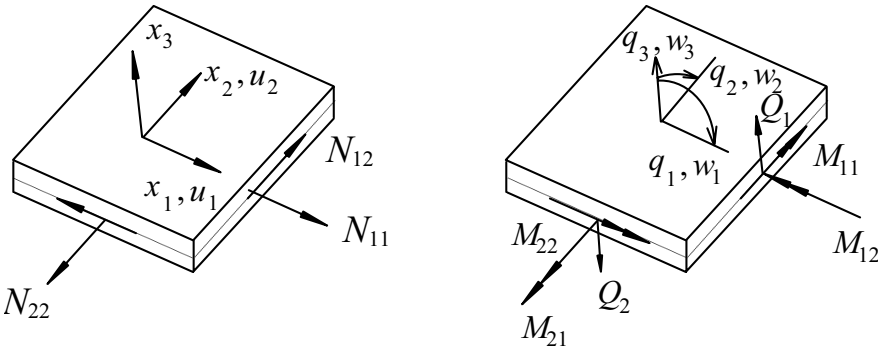


Figure 1: Sign convention for general displacements and tractions.

and plate bending problems as body forces in the deferential equations. Two numerical examples are presented and comparisons with the standard FEM software ABAQUS are made to demonstrate the accuracy and efficiency of the proposed method.

## 2 Deferential equations for Reissner-Mindlin plate bending theory

Consider an elastic plate of constant thickness $h$ with a domain $\Omega$ subjected to an in-plane transverse static load $q_0(\mathbf{x})$. The $x_1 - x_2$ plane is assumed to coincide with the mean surface of the plate. The Green's strain tensor for two-dimensional elasticity can be represented as [Wen and Aliabadi (2005)]

$$\varepsilon_{\alpha\beta} = \varepsilon^{(l)}_{\alpha\beta} + \varepsilon^{(n)}_{\alpha\beta} \tag{1}$$

where the subscripts $l$ and $n$ ($l$ and $n$ vary from 1 to 2) denote the linear and nonlinear contributions respectively. The linear term is defined as

$$\varepsilon^{(l)}_{\alpha\beta} = \frac{1}{2}(u_{\alpha,\beta} + u_{\beta,\alpha}) \tag{2}$$

and for the transverse shear strains

$$\varepsilon_{\alpha 3} = w_\alpha + w_{3,\alpha} \tag{3}$$

where $u_\alpha$ and $w_3$ are translation of displacements in $x_1$ and $x_2$ (two-dimensional elasticity) and $x_3$ directions respectively and $w_\alpha$ are rotations in $x_\alpha$ direction (see Figure 1). The nonlinear term in equation (1) is defined as

$$\varepsilon^{(n)}_{\alpha\beta} = \frac{1}{2} w_{3,\alpha} w_{3,\beta}. \tag{4}$$

Based on Hooke's law for two-dimensional plane stress, the membrane stress resultant-strain relationships can be written as follows:

$$\begin{aligned} N_{\alpha\beta} &= \frac{1-\nu}{2} B \Bigg( u_{\alpha,\beta} + u_{\beta,\alpha} + \frac{2\nu}{1-\nu} u_{\gamma,\gamma}\delta_{\alpha\beta} \\ &\qquad + w_{2,\alpha} w_{3,\beta} + \frac{2\nu}{1-\nu} w_{3,\gamma} w_{3,\gamma} \delta_{\alpha\beta} \Bigg) \\ &= N^{(l)}_{\alpha\beta} + N^{(n)}_{\alpha\beta} \end{aligned} \tag{5}$$

$$M_{\alpha\beta} = \frac{1-\nu}{2} D \left( w_{\alpha,\beta} + w_{\beta,\alpha} + \frac{2\nu}{1-\nu} w_{\gamma,\gamma}\delta_{\alpha\beta} \right) \tag{6}$$

where $B = Eh/(1-\nu^2)$ is tension stiffness, $D = Eh^3/12(1-\nu^2)$ denotes the plate stiffness, with $E$ as Young's modulus, $\nu$ as Poisson's ratio, and $\lambda^2 = 10/h^2$ is the shear correction factor in the Reissner theory. $N_{\alpha\beta}, Q_\alpha$ and $M_{\alpha\beta}$ are stress resultants for two-dimensional plane stress elasticity, shear force and bending moment stress resultants for plate bending problems. In the Reissner-Mindlin plate bending theory the equilibrium equations have the form [Mai-Duy et al (2007a)]

$$\begin{aligned} &N_{\alpha\beta,\beta} + b_\alpha = 0, \\ &M_{\alpha\beta,\beta} - Q_\alpha = 0, \\ &Q_{\alpha,\alpha} + q_3 = 0. \end{aligned} \tag{7}$$

The equilibrium equations can be written in terms of displacements as:

$$D^p_{\alpha\beta} u_\beta + b_\alpha = 0 \tag{8}$$

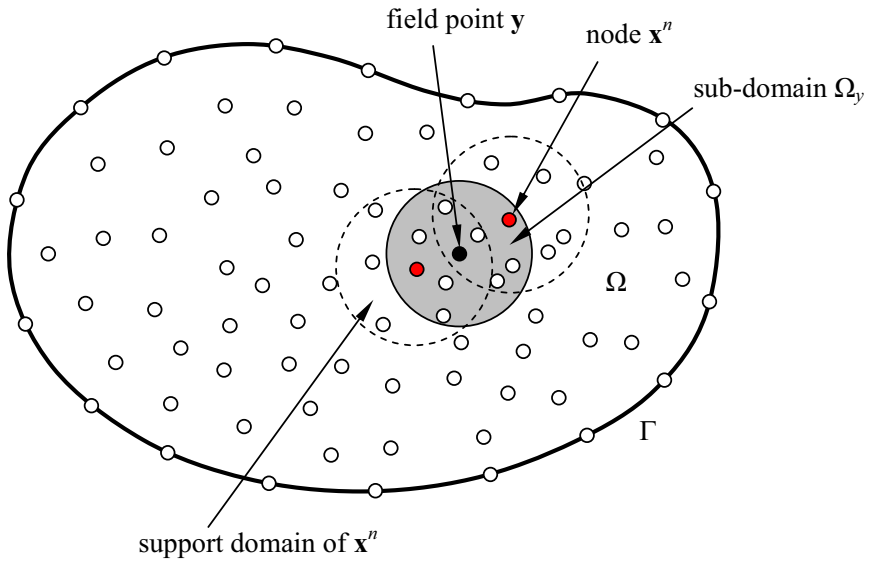


Figure 2: Sub-domain $\Omega_y$ for MLS approximation of the field point $\mathbf{y}$ and the support area around node $\mathbf{x}^n$.

for plane stress two-dimensional elasticity, and

$$D^b_{ik} w_k + q_i = 0 \tag{9}$$

for plate bending, where the Roman indices $\alpha$ and $\beta$ vary from 1 to 3 and the differential operators $D^p_{\alpha\beta}$ are defined, for plane stress elasticity, as

$$D^p_{\alpha\beta} = \frac{B}{2}(1-\nu)\delta_{\alpha\beta}\nabla^2 + \frac{B}{2}(1+\nu)\frac{\partial^2}{\partial x_\alpha \partial x_\beta} \tag{10}$$

with the equivalent body forces

$$b_\alpha = b^0_\alpha + N^{(n)}_{\alpha\beta,\beta} \tag{11}$$

where $b^0_\alpha$ denotes an applied body forces. The differential operators $D^b_{ik}$, for plate bending problems, are

$$\begin{aligned}
&D^b_{\alpha\beta} = \\
&\frac{D}{2}\left[(1-\nu)(\nabla^2-\lambda^2)\delta_{\alpha\beta} + (1+\nu)\frac{\partial^2}{\partial x_\alpha \partial x_\beta}\right] \\
&D^b_{\alpha 3} = -\frac{(1-\nu)D}{2}\lambda^2\frac{\partial}{\partial x_\alpha} \\
&D^b_{3\alpha} = -D^b_{\alpha 3} \\
&D^b_{33} = -\frac{(1-\nu)D}{2}\nabla^2
\end{aligned} \tag{12}$$

and the body forces

$$q_1 = q_2 = 0, \quad q_3 = q_0 + \left(N_{\alpha\beta} w_{3,\beta}\right)_{,\alpha} \tag{13}$$

in which $q_0$ represents the transverse load along the normal of the plate. The shear correction factor $\kappa^2$ in Mindlin's theory is usually taken as 5/6 in order for the two theories to coincide provided that $\lambda^2 = 12\kappa^2/h^2$. It is evident that the coupling terms are consisted in the nonlinear body force terms, i.e. $b_\alpha$ and $q_3$ in equations (11) and (13) and all of them should vanish for linear problem.

## 3 Meshless collocation method

### *3.1 Radial basis functions scheme*

The multiquadric radial basis function (MQRBF) was introduced by Hardy (1971) for multivariate interpolation of topographical surfaces. Since most radial basis functions are defined globally, the resulting matrix for interpolation is dense and can be highly ill-conditioned particularly for a large number of interpolation points. It also poses serious stability problems and is computationally inefficient. The conditionally positive definitiveness of various radial basis functions including MQRBF was investigated by Micchelli (1986) who provided a firm theoretical basis for large scale interpolation problems. The theoretical solvability proof on using the RBFs for solving PDEs has just been obtained by Hon and Schaback (2004). Recent applications using RBFs with local integral equation method for potential

problems in functionally graded anisotropic materials have been demonstrated by Sladek et al (2005).

The distribution of function $u$ in the sub-domain $\Omega_y$ over a number of randomly distributed notes $\{\mathbf{x}_i\}$, $i = 1,2,\ldots,n_y$ can be interpolated, at the point $\mathbf{y}$ by

$$u(\mathbf{y}) = \sum_{k=1}^{n_y} R_k(\mathbf{y},\mathbf{x})a_k = \mathbf{R}^T(\mathbf{y},\mathbf{x})\mathbf{a}(\mathbf{y}) \tag{14}$$

where $\mathbf{R}^T(\mathbf{y},\mathbf{x})=\{R_1(\mathbf{y},\mathbf{x}),R_2(\mathbf{y},\mathbf{x}),\ldots,R_{n(\mathbf{y})}(\mathbf{y},\mathbf{x})\}$ is the set of radial basis functions with centres placed around the point $\mathbf{y}$, $\{a_k\}_{k=1}^{n_y}$ are the unknown coefficients to be determined. The radial basis function selected multiquadrics [Atluri and Zhu (1999)] as

$$R_k(\mathbf{y},\mathbf{x}) = \sqrt{c^2 + |\mathbf{y}-\mathbf{x}_k|^2} \tag{15}$$

with a free parameter $c$. As the numerical result is very stable for the selection of this free parameter, we take $c = 1$ in all numerical examples as discussed in the paper of Zhu and Liu (1998). From the interpolation equation (15) a linear system for the unknowns coefficients $\mathbf{a}$ is obtained as

$$\mathbf{R}_0\mathbf{a} = \mathbf{u} \tag{16}$$

where

$$\mathbf{u}^T = \{u_1,u_2,\ldots,u_{n(\mathbf{y})}\} \tag{17}$$

are the nodal values and

$$\mathbf{R}_0(\mathbf{x}) = \begin{bmatrix} R_1(x_1) & R_2(x_1) & \ldots & R_{n(\mathbf{y})}(x_1) \\ R_1(x_2) & R_2(x_2) & \ldots & R_{n(\mathbf{y})}(x_2) \\ \vdots & \vdots & \ddots & \vdots \\ R_1(x_{n(\mathbf{y})}) & R_2(x_{n(\mathbf{y})}) & \ldots & R_{n(\mathbf{y})}(x_{n(\mathbf{y})}) \end{bmatrix}. \tag{18}$$

It is evident that the interpolation of field variable is satisfied exactly at each node. If the RBFs are positive definite, the matrix $\mathbf{R}_0$ can be assured to be invertible. Therefore, we can obtain the vector of unknowns from Eq. (16)

$$\mathbf{a} = \mathbf{R}_0^{-1}(\mathbf{x})\mathbf{u}(\mathbf{x}) \tag{19}$$

so that the approximation $u(\mathbf{y})$ can be represented, at domain point $\mathbf{y}$, as

$$u(\mathbf{y}) = \mathbf{R}^T(\mathbf{y})\mathbf{R}_0^{-1}(\mathbf{x})\mathbf{u}(\mathbf{x}) = \mathbf{\Phi}(\mathbf{y},\mathbf{x})\mathbf{u} = \sum_{k=1}^{n_y}\phi_k u_k \tag{20}$$

where the nodal shape function are defined by

$$\mathbf{\Phi}(\mathbf{y},\mathbf{x}) = \mathbf{R}^T(\mathbf{y})\mathbf{R}_0^{-1}(\mathbf{x}). \tag{21}$$

It is worth noting that the shape function depends uniquely on the distribution of scattered nodes within the support domain and has the Kronecker Delta property. As the inverse matrix of coefficient $\mathbf{R}_0^{-1}(\mathbf{x})$ is only a function of distributed node $\mathbf{x}$ in the support domain, it is much simpler to evaluate the partial derivatives of the shape function. In order to obtain an unique solution of the interpolation problem, a polynomial term is added to the interpolation (14), giving

$$\begin{aligned} u(\mathbf{y}) &= \sum_{k=1}^{n_y} R_k(\mathbf{y},\mathbf{x})a_k + \sum_{j=1}^{t} P_j(\mathbf{y})b_j \\ &= \mathbf{R}_0(\mathbf{y},\mathbf{x})\mathbf{a} + \mathbf{P}(\mathbf{y})\mathbf{b} \end{aligned} \tag{22}$$

along with the constraints

$$\sum_{j=1}^{t} P_k(\mathbf{x}_j)a_j = 0, \quad 1 \le k \le t \tag{23}$$

where $\{P_k\}_{k=1}^{t}$ is a basis for $P_{m-1}$, the set of d-variate polynomials of degree $\le m-1$, and

$$t = \binom{m+d-1}{d} \tag{24}$$

is the dimension of $P_{m-1}$. A set of linear equations can be written, in the matrix form, as

$$\mathbf{R}_0\mathbf{a} + \mathbf{P}^T\mathbf{b} = \mathbf{u}, \mathbf{P}\mathbf{a} = \mathbf{0} \tag{25}$$

with the matrix defined by:

$$P(\mathbf{x}) = \begin{bmatrix} P_1(x_1) & P_2(x_1) & \ldots & P_t(x_1) \\ P_1(x_2) & P_2(x_2) & \ldots & P_t(x_2) \\ \vdots & \vdots & \ddots & \vdots \\ P_1(x_{n(y)}) & P_2(x_{n(y)}) & \ldots & P_t(x_{n(y)}) \end{bmatrix}. \tag{26}$$

Solving these equations in Eq. (23) gives

$$\begin{aligned}\mathbf{b} &= \left(\mathbf{P}^T\mathbf{R}_0^{-1}\mathbf{P}\right)^{-1}\mathbf{P}^T\mathbf{R}_0^{-1}\mathbf{u},\mathbf{a} \\ &= \mathbf{R}_0^{-1}\left[\mathbf{I}-\mathbf{P}\left(\mathbf{P}^T\mathbf{R}_0^{-1}\mathbf{P}\right)^{-1}\mathbf{P}^T\mathbf{R}_0^{-1}\right]\mathbf{u}\end{aligned} \tag{27}$$

where $\mathbf{I}$ denotes the identity matrix. Substituting the coefficients $\mathbf{a}$ and $\mathbf{b}$ from Eq. (27) into Eq. (22), we can obtain the approximation of the field function in terms of the nodal values

$$u(\mathbf{y}) = \sum_{k=1}^{n_y}\phi_k(\mathbf{y},\mathbf{x})u_k(\mathbf{x}). \tag{28}$$

It is clear that the coefficient $\mathbf{a}$ and $\mathbf{b}$ are functions of nodal positions $\mathbf{x}$ with nodal values $\mathbf{u}$. It will be much easier to evaluate the approximated function's derivatives, which will be shown in the next section. In addition, by numerical examples, the accuracy is shown to be the same by using MQRBF with/without these polynomials.

### 3.2 Direct technique for MQRBF scheme

Since the MQRBFs are infinitely differentiable, it is much simpler to evaluate the partial derivatives of the shape function. From Eq. (20), we have

$$u_{,k}(\mathbf{y}) = \Phi_{,k}(\mathbf{y},\mathbf{x})\mathbf{u} = \sum_{i=1}^{n_y}\phi_{i,k}u_i \tag{29}$$

where

$$\begin{aligned}\Phi_{,k}(\mathbf{y},\mathbf{x}) &= \mathbf{R}_{,k}^T(\mathbf{y})\mathbf{R}_0^{-1}(\mathbf{x}) \\ &= [R_{1,k}(\mathbf{y}),R_{2,k}(\mathbf{y}),\ldots,R_{n(y),k}(\mathbf{y})]\mathbf{R}_0^{-1}(\mathbf{x})\end{aligned} \tag{30}$$

and

$$R_{i,k}(\mathbf{y}) = \frac{y_k - x_k^i}{\sqrt{c^2+|\mathbf{y}-\mathbf{x}^i|^2}}. \tag{31}$$

For the second order derivative of shape function, simply we have

$$\begin{aligned}\Phi_{,kl}(\mathbf{y},\mathbf{x}) &= \mathbf{R}_{,kl}^T(\mathbf{y})\mathbf{R}_0^{-1}(\mathbf{x}) \\ &= [R_{1,kl}(\mathbf{y}),R_{2,kl}(\mathbf{y}),\ldots,R_{n(y),kl}(\mathbf{y})]\mathbf{R}_0^{-1}(\mathbf{x})\end{aligned} \tag{32}$$

where

$$R_{i,kl}(\mathbf{y}) = \frac{1}{\sqrt{c^2+|\mathbf{y}-\mathbf{x}^i|^2}}\left[\delta_{kl}-\frac{\left(y_k-x_k^i\right)\left(y_l-x_l^i\right)}{c^2+|\mathbf{y}-\mathbf{x}^i|^2}\right]. \tag{33}$$

### 3.3 Indirect technique for RBF shape function's derivatives

It is evident that the evaluation of the second order and higher order derivatives of the shape function is costly and complicated particularly for the meshless collocation method. To overcome this difficulty, we can evaluate the higher orders of derivative for the shape function in an alternative way. From Eq. (20), we have the first order derivative in terms of the nodal values as [Wen and Aliabadi (2007)]

$$u_{,k}(\mathbf{y}) = \Phi(\mathbf{y},\mathbf{x})\mathbf{u}_{,k} = \sum_{i=1}^{n_y}\phi_i(\mathbf{y},\mathbf{x})\hat{u}_{i,k} \tag{34}$$

and hence the second order derivative can be written as

$$u_{,kl}(\mathbf{y}) = \Phi_{,l}(\mathbf{y},\mathbf{x})\hat{\mathbf{u}}_{,k} = \sum_{i=1}^{n_y}\phi_{i,l}(\mathbf{y},\mathbf{x})\hat{u}_{i,k}. \tag{35}$$

Considering the first derivative of the shape function, we obtain

$$\begin{aligned}u_{,kl}(\mathbf{y}) &= \Phi_{,l}(\mathbf{y},\mathbf{x})\hat{\mathbf{u}}_{,k} = \Phi_{,l}(\mathbf{y},\mathbf{x})\Phi_{,k}(\mathbf{x},\mathbf{x}')\hat{\mathbf{u}} \\ &= \sum_{i=1}^{n_y}\phi_{i,l}(\mathbf{y},\mathbf{x}^i)\sum_{j=1}^{n_y}\phi_{j,k}(\mathbf{x}^i,\mathbf{x}^j)\hat{u}_j\end{aligned} \tag{36}$$

This technique can be easily extended to higher order derivatives $u_{,k..pq..l}(\mathbf{y})$of the shape function directly. For instance, for the third order derivative, we have

$$\begin{aligned}&u_{,kql}(\mathbf{y}) \\ &= \Phi_{,l}(\mathbf{y},\mathbf{x})\Phi_{,q}(\mathbf{x},\mathbf{x}')\hat{\mathbf{u}}_{,k} \\ &= \Phi_{,l}(\mathbf{y},\mathbf{x})\Phi_{,q}(\mathbf{x},\mathbf{x}')\Phi_{,k}(\mathbf{x}',\mathbf{x}'')\hat{\mathbf{u}} \\ &= \sum_{i=1}^{n_y}\sum_{p=1}^{n_y}\sum_{j=1}^{n_y}\phi_{i,l}(\mathbf{y},\mathbf{x}^i)\phi_{p,q}(\mathbf{x}^i,\mathbf{x}^p)\phi_{j,k}(\mathbf{x}^p,\mathbf{x}^j)\hat{u}_j\end{aligned} \tag{37}$$

From the above relationship it can be seen that higher order derivatives of the shape function can be simply written in terms of the first order derivative.

### 3.4 Meshless collocation method

Consider a general partial differential equation for two-dimensional problem. We have the following

governing equations with certain given boundary conditions as:

$$\begin{aligned} D^p_{\alpha\beta}u_\beta(\mathbf{y}) &= b_\alpha(\mathbf{y}) \\ D^b_{ik}w_k(\mathbf{y}) &= b_k(\mathbf{y}) \quad \text{for } \mathbf{y}\in\Omega(\text{domain}) \\ u_\alpha(\mathbf{y}) &= \overline{u}_\alpha(\mathbf{y}) \\ w_i(\mathbf{y}) &= \overline{w}_i(\mathbf{y}) \quad \text{for } \mathbf{y}\in\Gamma_u \text{ (boundary (displacement condition)} \\ h_{\alpha\beta}u_\beta(\mathbf{y}) &= \overline{t}_\alpha(\mathbf{y}) \\ g_{ik}w_k(\mathbf{y}) &= \overline{p}_i(\mathbf{y}) \quad \text{for } \mathbf{y}\in\Gamma_\sigma \text{ (boundary traction condition)} \end{aligned} \tag{38}$$

where $h_{\alpha\beta}$ and $g_{ik}$ are differential operators (consist the first order derivatives of the shape functions) imposed as boundary conditions such as the relationships between stress and displacement (or moment and deflection) for the two-dimensional elasticity (or plate bending), $\overline{u}_\alpha, \overline{w}_i, \overline{t}_\alpha(=N_{\alpha\beta}n_\beta)$ and $\overline{p}_i(\overline{p}_\alpha = M_{\alpha\beta}n_\beta \text{ for } \alpha=1,2;\ \overline{p}_3 = Q_\beta n_\beta)$ represent the displacement and the traction values on the boundary, where $n_\beta$ denotes the component of outward unit normal to the boundary. By substituting Eq. (20) and collocating at $N_\Omega$ internal and $N_\Gamma(=N_{\Gamma_u}+N_{\Gamma_\sigma})$ boundary points, we have

$$\begin{aligned} \sum_{n=1}^{n_y^j} D^p_{\alpha\beta}\phi_n(\mathbf{y}^j,\mathbf{x}^n)\hat{u}^n_\beta &= b_\alpha(\mathbf{y}^j) \quad \alpha=1,2 \\ \sum_{n=1}^{n_y^j} D^b_{ik}\phi_n(\mathbf{y}^j,\mathbf{x}^n)\hat{w}^n_k &= q_i(\mathbf{y}^j) \quad i=1,2,3; \\ & \qquad j=1,2,\ldots,N_\Omega \end{aligned} \tag{39}$$

for the domain collocation points, and

$$\begin{aligned} \sum_{n=1}^{n_y^j} \phi_n(\mathbf{y}^j,\mathbf{x}^n)\hat{u}^n_\alpha &= \overline{u}_\alpha(\mathbf{y}^j) \quad \alpha=1,2 \\ \sum_{n=1}^{n_y^j} \phi_n(\mathbf{y}^j,\mathbf{x}^n)\hat{w}^n_i &= \overline{w}_i(\mathbf{y}^j) \quad i=1,2,3; \\ & \qquad j=1,2,\ldots,N_{\Gamma_u} \\ \sum_{n=1}^{n_y^j} h_{\alpha\beta}\phi_n(\mathbf{y}^j,\mathbf{x}^n)\hat{u}^n_\beta &= \overline{t}_\alpha(\mathbf{y}^j) \quad \alpha=1,2 \\ \sum_{n=1}^{n_y^j} g_{ik}\phi_n(\mathbf{y}^j,\mathbf{x}^n)\hat{u}^n_k &= \overline{p}_i(\mathbf{y}^j) \quad i=1,2,3; \\ & \qquad j=1,2,\ldots,N_{\Gamma_\sigma} \end{aligned} \tag{40}$$

for the boundary points. Thus the meshless collocation method can be carried out by solving a set of linear equations in (40) for static and dynamic elasticity problems. The total number of nodal values $\hat{u}_\alpha(\mathbf{y}^j)$ and $\hat{w}_k(\mathbf{y}^j)$ is $5(N_\Omega+N_{\Gamma_u}+N_{\Gamma_\sigma})$ for two-dimensional plate bending problems. The coupling of two-dimensional plane and plate bending problems occur in the body forces in equations (11) and (13). Solving these nonlinear equations gives the displacements $u_\alpha$ and deflections $w_i$ at any point including domain and boundary.

## 4 Numerical schemes for nonlinear equation systems

Considering the boundary condition with Eq. (43) by RBFs interpolation, a set of $2\times N$ linear algebraic equations can be obtained for two-dimensional in-plane elasticity and can be written in the matrix form as

$$\mathbf{D}^p\mathbf{u} = \mathbf{b} \tag{41}$$

where the matrix $\mathbf{D}^p$ consists of derivatives of the shape function and $\mathbf{b}$ is a nonlinear function of deflection $b^0_\alpha + N^{(n)}_{\alpha\beta,\beta}$. Similarly to the plate bending, a set of $3\times N$ algebraic equation can be written in matrix form as

$$\mathbf{D}^b\mathbf{w} = \mathbf{q} \tag{42}$$

where $\mathbf{D}^b$ denotes the coefficient matrix and $\mathbf{q}$ presents the nodal force vector and is a nonlinear function of membrane force and deflection, i.e. $q^0_3 + (N_{\alpha\beta}w_{3,\beta})_{,\alpha}$. To solve these two nonlinear systems, two numerical algorithms are proposed as follows:

### *4.1 Incremental load algorithm (LIA)*

Step 1: Let $m=1$, $q^m_3 = \Delta q_0$ (where $\Delta q_0$ is constant increment of transverse load) and

nonlinear terms in body forces $b_\alpha^{(n),m} = q_3^{(n),m} = 0$;

Step 2: Establish two linear algebraic systems for two-dimensional elasticity and plate bending respectively; solve these two systems in (11) and (13); and calculate the membrane forces $N_{\alpha\beta}$ and derivatives $w_{3,\alpha}$ in the domain;

Step 3: Evaluate all nonlinear terms and their derivatives, i.e. $[N_{\alpha\beta}^{(n)}]_{,\beta}^m$ and $[N_{\alpha\beta}w_{3,\beta}]_{,\alpha}^m$, and calculate the nonlinear body forces;

Step 4: If applied transverse load $q_3^m = q_0$, then go to Step 5, otherwise, let $m = m+1$ and $q_3^m = m\Delta q_3^0$ and go to Step 2;

Step 5: Output results for each step and terminate.

### 4.2 Full load algorithm (FLA)

Step 1: Let $m = 1$, $q_3^m = q_0$ and nonlinear terms in body forces $b_\alpha^{(n),m} = q_3^{(n),m} = 0$;

Step 2: Establish two linear algebraic systems for two-dimensional elasticity and plate bending respectively; solve these two systems in (11) and (13); and calculate the membrane forces $N_{\alpha\beta}$ and derivatives $w_{3,\alpha}$ in the domain;

Step 3: If $m \geq 2$ and relative error $\left|w_{3,\max}^m - w_{3,\max}^{m-1}\right| / \left|w_{3,\max}^m\right| \leq \varepsilon$ or $m \geq M$, where $\varepsilon$ is small value and $M$ is large number, then go to Step 6;

Step 4: Evaluate all nonlinear terms and their derivatives, i.e. $[N_{\alpha\beta}^{(n)}]_{,\beta}^m$ and $[N_{\alpha\beta}w_{3,\beta}]_{,\alpha}^m$, and calculate the nonlinear body forces;

Step 5: Let $m = m + 1$and update the nonlinear body forces by $q_3^m = q_3^0 + [q_3^{(n),m-1} + q_3^{(n),m-2}]/2$ and $b_\alpha^{(n),m} = [b_\alpha^{(n),m-1} + b_\alpha^{(n),m-2}]/2$. Go to Step 2;

Step 6: Output results and terminate.

In the first algorithm [Chen et al (2006)], load increment technique is used and the nonlinear body forces are evaluated directly by using the results from previous step. Therefore, this technique is simple and there are no iteration process needed. However, the numerical solutions for the final step depend on the history of the increment of loading. Iteration technique is involved in the second algorithm for full load process and save CPU time significantly compared with the first algorithm. The accuracy and convergence comparisons are made by considering the numerical examples in the following section. Numerical computations indicated that it only takes 4 to 5 iterations for the nonlinear scheme to converge to the solution.

## 5 Numerical examples

In the following numerical demonstrations, Young's modulus $E$ is selected as $10^7$ and Poisson's ratio $\nu$=0.316. The radius of local subdomain $d_y$ centred at the field point is determined by the minimum number of collocation points in the sub-domain $n_y > 15$. The normalized increment of transverse load $\Delta q = 0.2q_0a^4/Eh^4$ for incremental load algorithm (IL) and$\varepsilon = 0.01$ for full load algorithm (FL). In addition, 441 (21×21) uniformly distributed nodes are selected in the domain.

### 5.1 Clamped and simply supported and square plate under uniform load

Consider a square plate of width $a$ and height $h$ as shown in Figure 3. For the clamped boundary condition, the displacement and traction are defined as

$$\begin{aligned} &\overline{u}_1 = \overline{u}_2 = \overline{w}_1 = \overline{w}_2 = \overline{w}_3 = 0 \quad x_1 = \pm a/2 \\ &\overline{u}_1 = \overline{u}_2 = \overline{w}_1 = \overline{w}_2 = \overline{w}_3 = 0 \quad x_2 = \pm a/2; \end{aligned} \tag{43}$$

and for simply supported boundary condition

$$\begin{aligned} &\overline{u}_1 = \overline{u}_2 = \overline{w}_2 = \overline{w}_3 = \overline{p}_1 = 0 \quad x_1 = \pm a/2 \\ &\overline{u}_1 = \overline{u}_2 = \overline{w}_1 = \overline{w}_3 = \overline{p}_2 = 0 \quad x_2 = \pm a/2. \end{aligned} \tag{44}$$

The ratios $h/a$ are selected as 0.05 and 0.1 for moderate and thick plate respectively. The indirect technique to evaluate high order derivatives of shape functions is employed in this example.

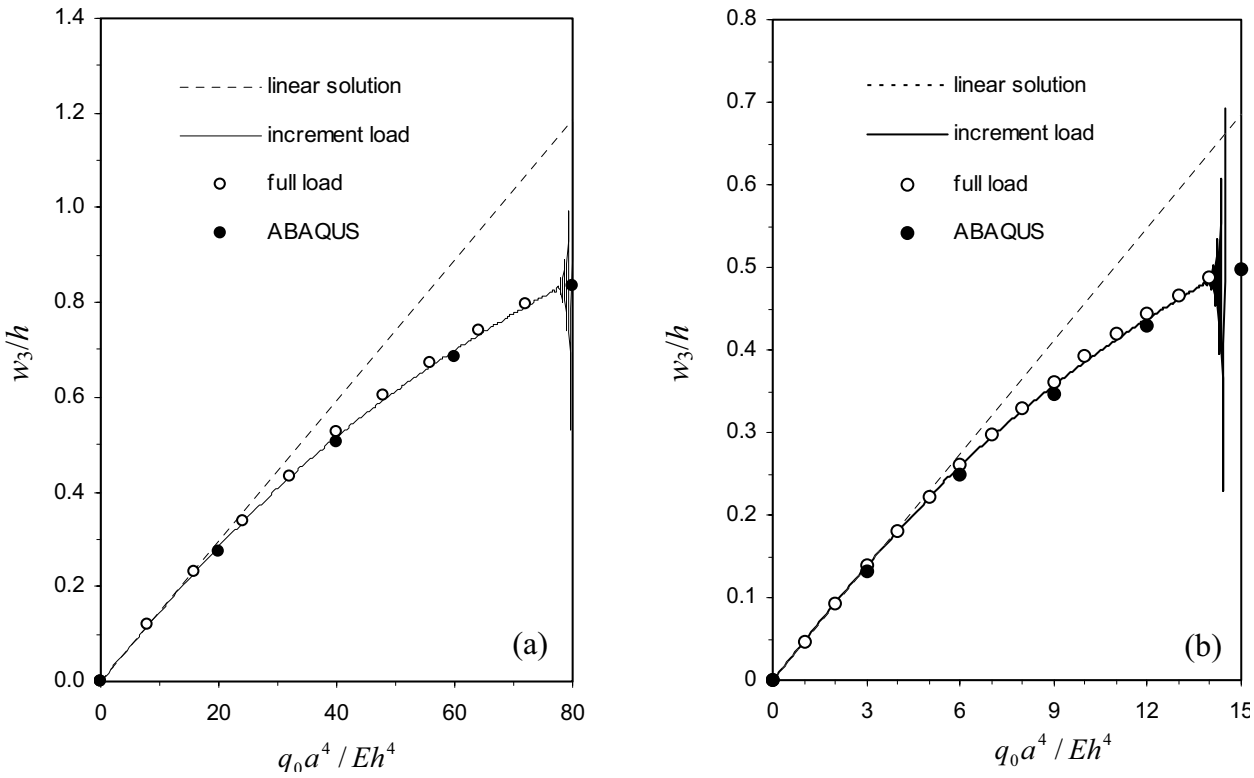


Figure 3: Normalized maximum deflection $w_3/h$ at the centre of plate subjected to uniform load various with normalized applied load $q_0a^4/Eh^4$ for (a) clamped boundary condition; (b) simply supported boundary condition, where $h/a$=0.05.

To study the convergence of the method, two regular node distributions with 441 and 961 nodes are used for the RBF approximation of quantities. We observe that the convergences for both quantities are almost the same. The normalized maximum deflections of plate at centre point $w_{\max}/h$ are plotted in Figures 3 and 4 against the normalized transverse load $q_0a^4/Eh^4$. For full load algorithm (FL), the number of iterations is less than 10 in general. Figure 5 shows the accuracy and convergence of the FL for each iteration step when $q_0a^4/Eh^4 = 40$, $h/a$=0.05 and $\varepsilon$=0.001 for clamped boundary case. For each figure, the results by using the two algorithms, i.e. IL and FL, are given in for comparison. For larger normalized transverse load $q_0a^4/Eh^4$, the solutions both for IL and FL are divergent and isolation of deflection occurs. This is due to the errors induced by each step of load increment (assumption of linearization in each step). A good agreement between the results from the standard finite element software (ABAQUS) and the proposed algorithms has been achieved, which also verifies the accuracy of the proposed meshless computational method. For the same accuracy, the CPU time used by IL is much higher than that by FL.

We also made comparisons for deflections and stresses in the field of plate with ABAQUS in Figures 6 and 7 respectively. The deflection contours of $w_3$ and in-plane displacement $u_1$ of plate are plotted in Figure 6 and the stresses contours of $\sigma_{11}$ on the top and bottom surfaces of plate in Figure 7, where we select $h/a$=0.1 and $q_0a^4/Eh^4 = 50$. The agreement with the results of ABAQUS is also excellent. However, the accuracy of displacement and deflection are higher than stresses.

### *5.2 Clamped square plate with variable thickness under uniform load*

Consider a clamped square plate with varying thickness which is a function of coordinate as shown in Figure 8. The thickness can be written

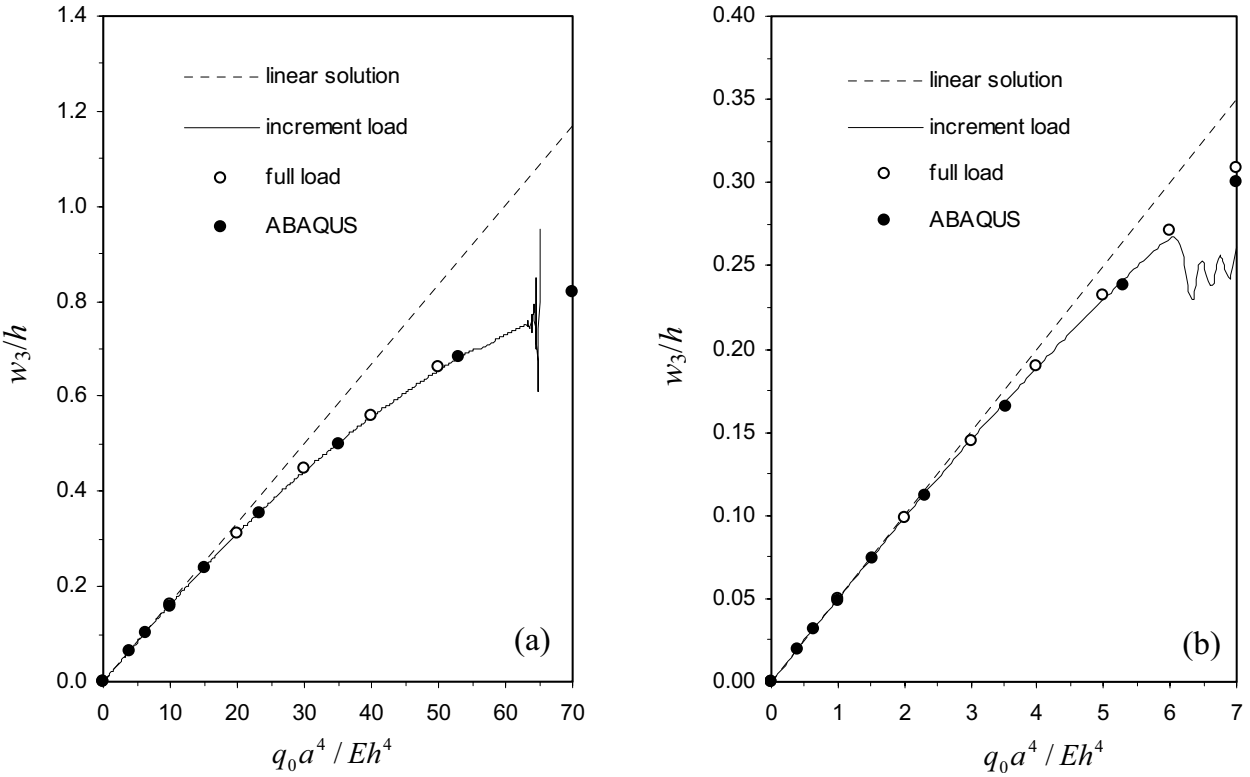


Figure 4: Normalized maximum deflection $w_3/h$ at the centre of plate subjected to uniform load various with normalized applied load $q_0a^4/Eh^4$ for (a) clamped boundary condition; (b) simply supported boundary condition, where $h/a$=0.1.

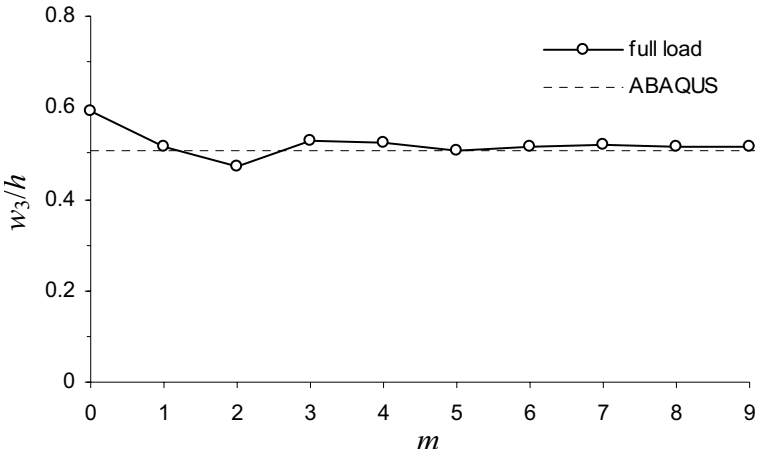


Figure 5: Demonstration of convergence for the full load algorithm when $q_0a^4/Eh^4$=40 and $h/a$=0.05, $m$ is the step of iteration.

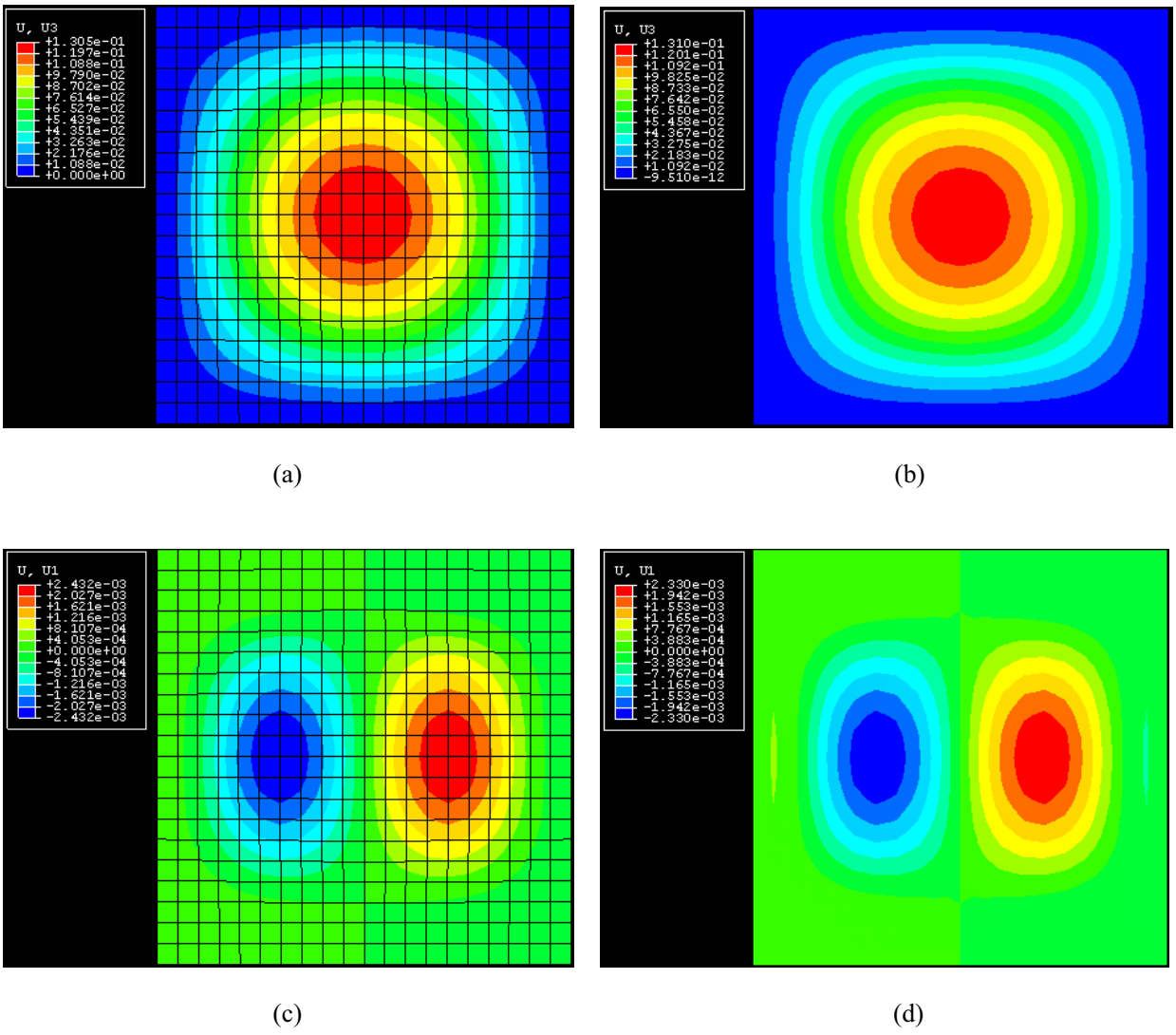


Figure 6: Comparison with finite element method and meshless method (RBF) for a square clamped moderate thick plate ($h/a$=0.1) with uniform pressure $q_0a^4/Eh^4$=50: (a) contour of deflection $w$ of plate by ABAQUS; (b) contour of deflection $w$ by RBF; (c) contour of in-plane displacement $u$ by ABAQUS; (d) contour of in-plane displacement $u$ by RBF. The unit for the deflection and displacement is meter.

as

$$h(x_1,x_2)=h_0+\frac{h_1-h_0}{a}x_1 \quad 0\le x_1\le a,\ 0\le x_2\le a. \tag{45}$$

The equilibrium equations in terms of displacements are obtained, for the domain collocation points, as follows:

$$D(x_1)\nabla^2 w_1+\frac{D(x_1)}{2}(1+\nu)\frac{\partial}{\partial x_2}\left(-\frac{\partial w_1}{\partial x_2}+\frac{\partial w_2}{\partial x_1}\right)$$
$$-C(x_1)w_1-C(x_1)\frac{\partial w_3}{\partial x_1}+\frac{\partial D}{\partial x_1}\left(\frac{\partial w_1}{\partial x_1}+\nu\frac{\partial w_2}{\partial x_2}\right)$$
$$=0$$
$$D(x_1)\nabla^2 w_2+\frac{D(x_1)}{2}(1+\nu)\frac{\partial}{\partial x_1}\left(\frac{\partial w_1}{\partial x_2}-\frac{\partial w_2}{\partial x_1}\right)$$
$$-C(x_1)w_2-C(x_1)\frac{\partial w_3}{\partial x_2}$$
$$+(1+\nu)\frac{\partial D}{\partial x_1}\left(\frac{\partial w_1}{\partial x_2}+\frac{\partial w_2}{\partial x_1}\right)=0$$
$$C(x_1)\nabla^2 w_3+C(x_1)\left(\frac{\partial w_1}{\partial x_1}+\frac{\partial w_2}{\partial x_2}\right)$$

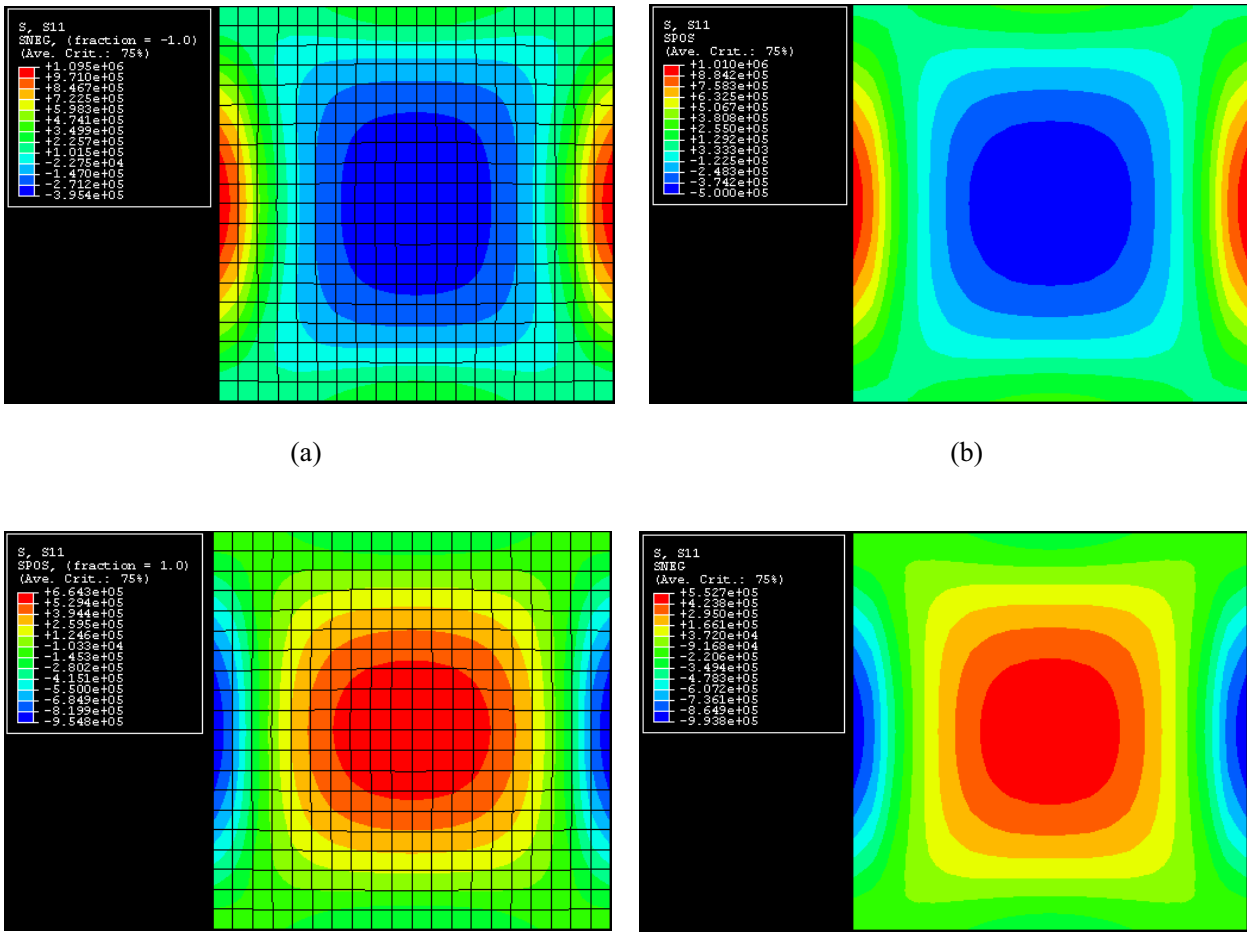


Figure 7: Comparison of stress $\sigma_{xx}$ on the top and bottom surfaces with finite element method and meshless method (RBF) for a square clamped moderate thick plate ($h/a$=0.1) with uniform pressure $q_0a^4/Eh^4$=50: (a) contour of stress by ABAQUS on the top surface; (b) contour of stress by RBF on the top surface; (c) contour of stress on the bottom surface by ABAQUS; (d) contour of stress by RBF on the bottom surface. The unit for the deflection and displacement is Pa (N/mm$^2$).

$$+\frac{\partial C}{\partial x_1}\left(w_1+\frac{\partial w_3}{\partial x_1}\right)+q_3=0 \tag{46}$$

for the plate bending and

$$\begin{aligned}
&B(x_1)\nabla^2 u_1+\frac{B(x_1)}{2}(1+\nu)\frac{\partial}{\partial x_2}\left(-\frac{\partial u_1}{\partial x_2}+\frac{\partial u_2}{\partial x_1}\right)\\
&+\frac{\partial B}{\partial x_1}\left(\frac{\partial u_1}{\partial x_1}+\nu\frac{\partial u_2}{\partial x_2}\right)+b_1=0\\
&B(x_1)\nabla^2 u_2+\frac{B(x_1)}{2}(1+\nu)\frac{\partial}{\partial x_1}\left(\frac{\partial u_1}{\partial x_2}-\frac{\partial u_2}{\partial x_1}\right)\\
&+(1-\nu)\frac{\partial B}{\partial x_1}\left(\frac{\partial u_1}{\partial x_2}+\frac{\partial u_2}{\partial x_1}\right)+b_2=0
\end{aligned} \tag{47}$$

for two-dimensional elasticity, in which

$$\begin{aligned}
D(x_1)&=Eh^3(x_)/12(1-\nu^2),\\
B(x_1)&=Eh(x_1)/(1-\nu^2)
\end{aligned} \tag{48}$$

and

$$\begin{aligned}
\frac{\partial D}{\partial x_1}&=\frac{Eh^2(x_1)}{4(1-\nu^2)}\frac{h_1-h_0}{a},\\
\frac{\partial C}{\partial x_1}&=\frac{5E}{12(1+\nu)}\frac{h_1-h_0}{a},\\
\frac{\partial B}{\partial x_1}&=\frac{E}{(1-\nu^2)}\frac{h_1-h_0}{a}.
\end{aligned} \tag{49}$$

On the boundary, the operators $h_{\alpha\beta}$ and $g_{ik}$ are the

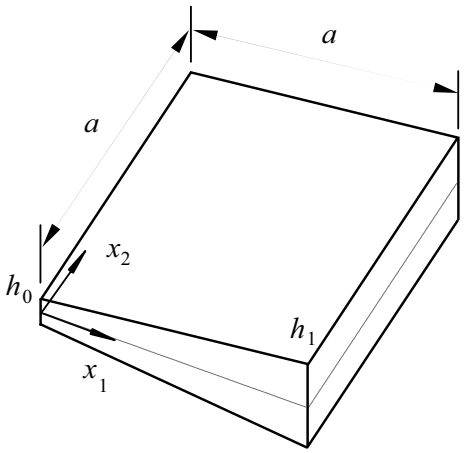


Figure 8: A square plate with varying thickness.

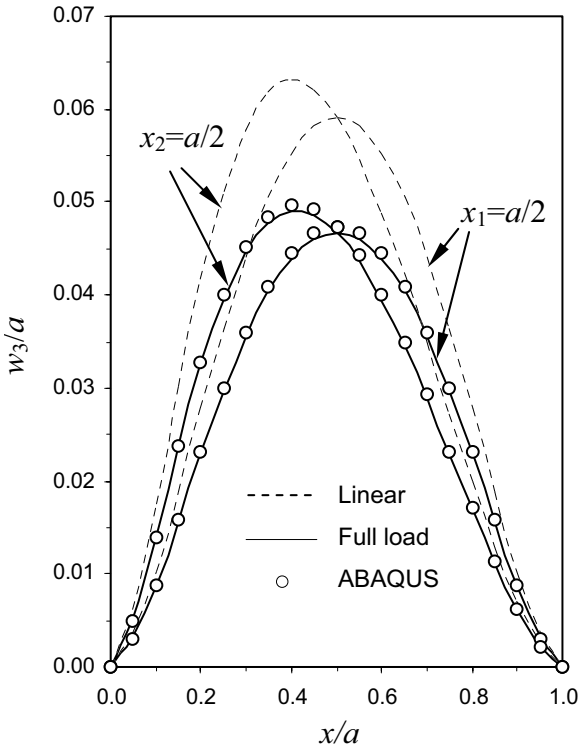


Figure 9: Deflections and comparison with finite element method for a square clamped moderate various thick plate with uniform pressure $q_0a^4/Eh^4$=250, $h_0/a$=0.05, $h_1/a$=0.1.

same as presented in Eq.(38). The ratios $h_0/a$ and $h_1/a$ are selected as 0.05 and 0.1 respectively in this example and the normalized transverse load $q_0a^4/Eh_0^4 = 250$. Using the full load algorithm, we present the normalized deflections of plate $w_{\max}/a$ on the geometry symmetric lines $x_1 = 0$ or $x_2 = 0$ in Figures 9. The results by ABAQUS are also plotted in this figure for comparison. It is reasonably observed that the maximum deflection point shifts to the left hand side from the center of the plate due to the effect of the variation of thickness. Comparison has shown the high accuracy of the proposed meshless computational method and demonstrated its flexibility and simplicity for treating these kinds of complex problems.

## 6 Conclusions

This paper presented the application of the meshless computational method to large deformation of Reissner-Mindlin plate with two algorithms (load increment algorithm and full load algorithm) to solve nonlinear equations. The advantage of using the meshless collocation method is to interpolate accurately higher order derivatives of shape functions at no cost on extra-interpolation. An indirect method has also been developed and shown to be economic and efficient for approximating any order derivatives of shape function in terms of the first derivative matrix. From the results of numerical verification, we observe that the proposed meshless computational method by using RBF interpolation is efficient to handle large deformation problems for Reissner-Mindlin plate. One of the main advantages is its simplicity for computational implementation. Contrary to the conventional boundary integral equation method, it requires no integrals and fundamental solutions to formulate the system equations. It has been shown that the meshless method provides a flexible and simple method and suitable for certain complicated partial linear and nonlinear differential equations such as dynamic orthotropic moderate thick plate, functionally graded materials, Winkler elastic foundation and etc. The disadvantage of using the meshless method is also evident such as more collocation points needed for accurate solution and stability for large applied load.

**Acknowledgement:** The work described in this paper was fully supported by a grant from CityU

7001646.

## References

**Atluri, S. N.** (2004): *The Meshless Method (MLPG) for Domain and BIE Discretizations*, Forsyth, GA, USA, Tech Science Press.

**Atluri, S. N.; Shen, S.** (2002): The meshlesss local Peyrov-Galerkin (MLPG) method: a simple and less-costly alternative to the finite element and boundary element method, *CMES: Computer Modeling in Engineering and Sciences*, **3**, 11-52.

**Atluri, S. N.; Zhu, T.** (1998a): A new meshless local Peyrov-Galerkin (MLPG) approach to nonlinear problems in computational modelling and simulation, *Comput. Model Simul. Engng.*, **3**, 187-196.

**Atluri, S. N.; Zhu, T.** (1998b): A new meshless local Peyrov-Galerkin (MLPG) approach in computational mechanics, *Comput. Mech.*, **22**, 117-127.

**Atluri, S. N.; Zhu, T.** (1999): The meshlesss local Peyrov-Galerkin (MLPG) approach for solving problems in elasto-statics, *Comput. Mech.*, **25**, 169-179.

**Belytschko, T.; Lu, Y. Y.; Gu, L.** (1994): Element-free Galerkin method, *Int. J. Numerical Methods in Engineering*, **37**, 229-256.

**Chantasiriwan, S.** (2006): Performance of multiquadric collocation method in solving lid-driven cavity flow problem with low Reynolds number, *CMES: Computer Modeling in Engineering and Sciences*, **15**, 137-146.

**Chen, J. T.; Wu, C. S.; Chen, K. H.; Lee, Y. T.** (2006): Degenerate scale for analysis of circular plate using the boundary integral equations and boundary element method, *Comput. Mech.*, **38**, 33-49.

**Hardy, R. L.** (1971): Multiquadric equations of topography and other irregular surface, *J. Geophys. Res.*, **76**, 1905-1915.

**Hon, Y. C.; Cheung, K. F.; Mao, X. Z.; Kansa, E. J.** (1999): A Multiquadric Solution for the Shallow Water Equations, *ASCE Journal of Hydraulic Engineering*, **125**, 524-533.

**Hon, Y. C.; Ling, L.; Liew, K. M.** (2005): Numerical analysis of parameters in a laminated beam model by radial basis functions, *CMC: Computers, Materials and Continua*, **2**, 39-49.

**Hon, Y. C.; Schaback, R.** (2004): Solvability of partial differential equations by meshless kernel methods, *Advances in Computational Mathematics*, online first.

**Hon, Y. C.; Wu, Z.** (2000): A numerical computation for inverse boundary determination problems, *Engineering Analysis with Boundary Elements*, **24**, 599-606.

**Kansa, E. J.** (1990): Multiquadric – a scattered data approximation scheme with applications to computational fluid-dynamics. I. Surface approximations and partial derivatives estimates, *Comput. Math. Appl.*, **19**, 127-145.

**La Rocca, A.; Power, H.; La Rocca V.; Morale M.** (2005): A meshless approach based upon radial basis function Hermite collocation method for predicting the cooling and the freezing times of foods, *CMC: Computers, Materials and Continua*, **2**, 239-250.

**Le, P.; Mai-Duy, N.; Tran-Cong, T.; Baker, G.** (2007): A numerical study of strain localization in elasto-thermo-viscoplastic materials using radial basis function networks, *CMC: Computers, Materials and Continua*, **5**, 129-150.

**Lei, X. Y.; Huang, M. K.; Wang, X. X.** (1990): Geometrically nonlinear analysis of a Reissner type plate by the boundary element method, *Comput. Struct.*, **37**, 911-916.

**Liu, W. K.; Jun, S.; Zhang, Y.** (1995): Reproducing kernel particle methods, *Int. J. Numerical Methods in Engineering*, **20**, 1081-1106.

**Mai-Cao, L.; Tran-Cong, T.** (2005): A meshless IRBFN-based method for transient problems, *CMES: Computer Modeling in Engineering and Sciences*, **7**, 149-172.

**Mai-Duy, N.; Khennane, A.; Tran-Cong, T.** (2007a): Computation of laminated composite plates using integrated radial basis function networks, *CMC: Computers, Materials and Continua*, **5**, 63-78.

**Mai-Duy, N.; Mai-Cao L.; Tran-Cong, T.** (2007b): Computation of transient viscous flows

using indirect radial basis function networks, *CMES: Computer Modeling in Engineering and Sciences*, **18**, 59-78.

**Micchelli, C. A.** (1986): Interpolation of scattering data: distance matrices and conditionally positive definite functions, *Constructive Approximation*, **2**, 11-22.

**Mindlin, R. D.** (1951): Influence of rotary inertia and shear on flexural motions of isotropic, elastic plates. *Journal of Applied Mechanics ASME*, **18**, 31-38.

**Nardini, D.; Brebbia, C. A.** (1982): A new approach to free vibration analysis using a boundary element method, in Boundary Element Methods in Engineering, edited by C. A. Brebbia, 312-326.

**Nayroles, B.; Touzot, G.; Villon, P.** (1992): Generalizing the finite element method: diffuse approximation and diffuse elements, *Computational Mechanics*, **10**, 307-318.

**Reissner, E.** (1945): The effect of transverse shear deformation on the bending of elastic plates. *Journal of Applied Mechanics ASME*, **12**, A69-A77.

**Šarler, B.** (2005): A radial basis function collocation approach in computational fluid, *CMES: Computer Modeling in Engineering and Sciences*, **7**, 185-194.

**Sladek, J.; Sladek, V.; Atluri, S. N.** (2004a): Meshless Local Petrov-Galerkin method for heat conduction problem in an anisotropic medium, *CMES: Computer Modeling in Engineering and Sciences*, **6**, 309-318.

**Sladek, J.; Sladek, V.; Zhang, CH.** (2004b): Heat conduction analysis in nonhomogeneous anisotropic solid, ZH Yao, MW Yuan, WX Zhong edited, Computational Mechanics, Tsinghua University Press and Springer, 609-614.

**Sladek, J.; Sladek, V.; Tanaka, M.; Zhang, CH.** (2005): Local integral equation method for potential problems in functionally graded anisotropic materials, *Engineering Analysis with Boundary Elements*, **29**, 829-843.

**Shu, C.; Ding, H.; Yeo, K. S.** (2005): Computation of incompressible Navier-Stokes equations by local RBF-based differential quadrature method, *CMES: Computer Modeling in Engineering and Sciences*, **7**, 195-206.

**Vander Ween, F.** (1982): Application of the boundary integral equation method to Reissner's plate model. *International Journal for Numerical Methods in Engineering*, **18**, 1-10.

**Wang, W.; Ji, X.; Tanaka, M.** (2000): A dual reciprocity boundary element approach for the problems of large deflection of thin elastic plates, *Comput. Mech.*, **26**, 58-65.

**Wen, P. H.; Aliabadi, M. H.** (2005): Large deformation analysis of Reissner plate by boundary element method, *Computers and Structure*, **83**, 870-879.

**Wen, P. H.; Aliabadi, M. H.** (2007): An Improved Meshless Collocation Method for Elastostatic and Elastodynamic Problems, *Computer Methods in Appl Mech and Engng* (in press).

**Wen, P. H.; Aliabadi, M. H.; Zhang, J. Z.** (2005): Displacement Discontinuity Method for Cracked Reissner Plate Analysis: Static and Dynamic, *International Journal of Fracture*, **135**, 97-118.

**Young, D. L.; Chen, C. S.; Wong, T. K.** (2006): Solution of Maxwell's equations using the MQ method, *CMC: Computers, Materials and Continua*, **4**, 267-276.

**Zhu, S. P.; Liu, H. W.** (1998): On the application of the generalized multiquadric bases in conjunction with the LTDRM to solve transient nonlinear diffusion equations, *Appl Math Comptut*, **96**, 161-175.